REPORT DOCUMENTATION PAGE

Form Approved
OMB No. 0704-0188

1. REPORT DATE *(DD-MM-YYYY)*	**2. REPORT TYPE**	**3. DATES COVERED** *(From - To)*
25-07-2012	Conference Paper	

4. TITLE AND SUBTITLE

Comparison of Numerical and Experimental Time-Resolved Near-Field Hall Thruster Plasma Properties

5a. CONTRACT NUMBER

5b. GRANT NUMBER

5c. PROGRAM ELEMENT NUMBER

6. AUTHOR(S)
Gonzales, A.E.; Scharfe, M.K.; Koo, J.W.; Hargus Jr., W.A.

5d. PROJECT NUMBER

5f. WORK UNIT NUMBER
23080535

7. PERFORMING ORGANIZATION NAME(S) AND ADDRESS(ES)

Air Force Research Laboratory (AFMC)
AFRL/RZSS
1 Ara Drive
Edwards AFB CA 93524-7013

8. PERFORMING ORGANIZATION REPORT NUMBER

9. SPONSORING / MONITORING AGENCY NAME(S) AND ADDRESS(ES)

Air Force Research Laboratory (AFMC)
AFRL/RQR
5 Pollux Drive
Edwards AFB CA 93524-7048

10. SPONSOR/MONITOR'S ACRONYM(S)

11. SPONSOR/MONITOR'S NUMBER(S)
AFRL-RZ-ED-TP-2012-227

12. DISTRIBUTION / AVAILABILITY STATEMENT

Approved for public release; distribution unlimited (PA #12625).

13. SUPPLEMENTARY NOTES
For presentation at the 48th AIAA/ASME/SAE/ASEE Joint Propulsion Conference & Exhibit and 10th International Energy Conversion Engineering Conference, Atlanta, GA, 29 July- 2 August 2012

14. ABSTRACT

The breathing mode of a xenon 600W Hall effect thruster has been studied using both temporally resolved experimental data and numerical modeling. Fluctuations in xenon neutral NIR (810-835 nm) emission in the near field thruster plume have been measured at 1 μs resolution using a high-speed intensified charge coupled device (ICCD). Oscillations in electron temperature, 3-9 eV, have been inferred using a collisional-radiative model and a two-line ratio method. The time-resolved emission and electron temperature measurements are then used to assess the accuracy of the numerical model HPHall. Simulations were found to be consistent with a -6 phase delay measured between discharge current and electron temperature cycles, but were unable to predict the magnitude of oscillations observed.

15. SUBJECT TERMS

16. SECURITY CLASSIFICATION OF:			**17. LIMITATION OF ABSTRACT**	**18. NUMBER OF PAGES**	**19a. NAME OF RESPONSIBLE PERSON**
					W.A. Hargus Jr.
a. REPORT	**b. ABSTRACT**	**c. THIS PAGE**			**19b. TELEPHONE NUMBER** *(include area code)*
Unclassified	**Unclassified**	**Unclassified**	SAR	18	N/A

AIAA Joint Propulsion Conference
July- Aug 2012, Atlanta, GA

Comparison of Numerical and Experimental Time-Resolved Near-Field Hall Thruster Plasma Properties

Ashley E. Gonzales, Michelle K. Scharfe, Justin W. Koo, William A. Hargus, Jr.
Air Force Research Laboratory, Edwards AFB, CA 93524

Abstract

The breathing mode of a xenon 600W Hall effect thruster has been studied using both temporally resolved experimental data and numerical modeling. Fluctuations in xenon neutral NIR (810-835 nm) emission in the near field thruster plume have been measured at 1 μs resolution using a high-speed intensified charge coupled device (ICCD). Oscillations in electron temperature, 3-9 eV, have been inferred using a collisional-radiative model and a two-line ratio method. The time-resolved emission and electron temperature measurements are then used to assess the accuracy of the numerical model HPHall. Simulations were found to be consistent with a -68° phase delay measured between discharge current and electron temperature cycles, but were unable to predict the magnitude of oscillations observed.

I. Introduction

Hall thrusters are a plasma propulsion technology widely used due to their low thrust, high specific impulse operation. With increasing demand for these thrusters to perform a wide range of missions, there is a need to move away from the costly experiment-based thruster development to a more efficient numerical modeling-based approach. Although models have been moderately successful at predicting thruster performance using basic operating principles[1-7], verification is needed to determine their ability to accurately model the more complex features of thruster operation.

Of particular interest is the low frequency (10-50 kHz) fluctuation in discharge current, often referred to in literature as the *breathing mode*[8,9]. The fluctuations are believed to be due to a periodic cycling of the neutral and plasma density in the exhaust region and are thought to have a strong influence on electron transport. Oscillations in plasma properties have been previously replicated in numerical modeling[1,4], but until recently, comparisons with temporally resolved experimental data were limited.

Time resolved measurements of the far plume have been made using a high-speed dual Langmuir probe (HDLP)[10,11]. Using rapid sweeps, measurements of electron density, electron temperature, and plasma potential were made on a μs timescale. However, probe measurements are limited to the far-field due to their interference with the plume. Optical measurements are an attractive non-intrusive alternative resolution on the ns temporal scale. These measurements are mainly limited by signal to noise ratio (SNR) and the speed of the optical components.

In this study, time-resolved optical measurements are used to assess the temporal fidelity of the numerical model HPHall[1]. Breathing mode oscillations in xenon neutral NIR emission are measured in the near field with a 1 μs resolution using a high speed ICCD and used to infer fluctuations in electron temperature using a collisional-radiative model[12]. Breathing mode simulations are completed using HPHall to characterize plasma oscillations. The measurements are then compared to the fluctuations predicted with HPHall assess the temporal fidelity of the model.

II. Experimental Measurements

Test Facility and Thruster

The measurements reported here were performed in vacuum Chamber 1 at the Air Force Research Laboratory at Edwards Air Force Base. This vacuum facility consists of a 2.4 m diameter, 4.1 m long cylindrical, non-magnetic stainless steel vacuum chamber with two liquid nitrogen baffled (76 K), 1.2 m flanged gaseous helium two stage cryogenic (15 K) vacuum pumps capable of pumping speeds of 48,500 L/s on xenon. A cold cathode gauge is used to determine a chamber background pressure of approximately 4 x 10^{-6} Torr (corrected for xenon) during thruster operation.

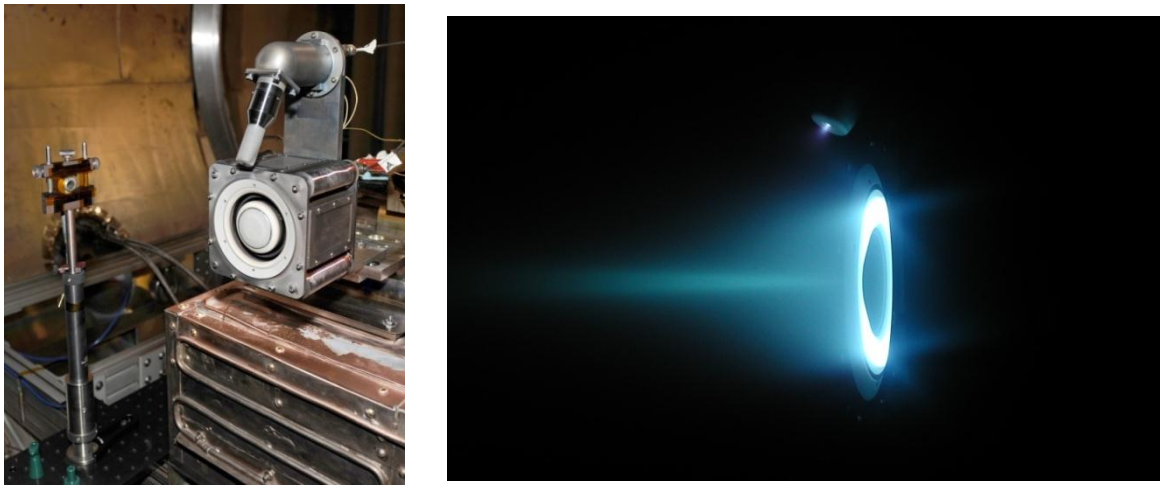

Figure 1: Photographs of BHT-600 Hall effect thruster. Left: Thruster shown with optical collection apparatus mounted to left. Collection volume taken 6 mm downstream of exit plane. Right: Thruster firing with Xe propellant, highlighting structure of near plume.

Table 1: BHT-600 Hall thruster at nominal xenon operating conditions and performance[13]

Parameter	Value
Anode Flow Rate	2.45 mg/s
Cathode Flow Rate	197 μg/s
Anode Potential	300 V
Anode Current	2.05 A
Magnetic Current (inner coils)	2.0 A
Magnetic Current (outer coils)	2.0 A

Thrust	39 mN
Specific Impulse	1530 s
Propulsive Efficiency	49%

The Hall effect thruster used in this study is a 600 W BHT-600 with a 3.2 mm hollow cathode manufactured by the Busek Company (Natick, MA) This thruster has been studied previously using both electrostatic probes and various optical diagnostics [12,14-16]. Photographs of the Chamber 1 apparatus and thruster firing are shown in Figure 1. The BHT-600 Hall effect thruster has an acceleration channel outer radius of 32 mm, an inner radius of 24 mm, and a 10 mm depth. The magnetic field is produced by four outer coils, and one inner magnetic coil. The outer and inner coil currents are independently adjustable for optimization of the field strength. The nominal conditions and performance of the BHT-600 as provided by the Busek Company are shown in Table 1[13].

A sample BHT-600 discharge current at nominal conditions is shown on the left in Figure 2. On the right, the frequency analysis shows a fundamental frequency of 38 kHz. The relatively small second harmonic indicates the oscillations are fairly sinusoidal. Although the amplitude of the signal varies, the period of the fluctuations remains consistent at 26.4± 0.3 μs based on the half width at half maximum (HWHM) of the FFT trace.

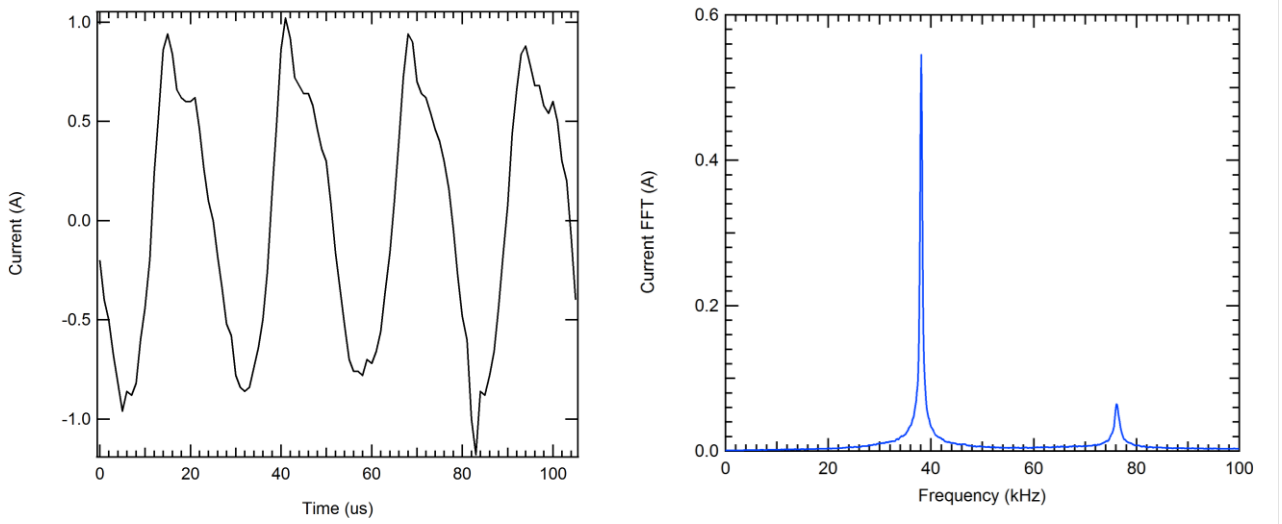

Figure 2: BHT-600 discharge current oscillations at nominal conditions. Left: AC portion of thruster discharge current. Right: Discharge current FFT trace, breathing mode frequency = 38 kHz.

Emission Measurements

The optical system used to measure the emission spectrum is schematically shown Figure 3. Plume emission is collected at a single location 6 mm downstream of the thruster exit plane using a 6 mm diameter reflective fiber optic beam coupler. The beam coupler focuses a 6 mm diameter beam onto the optical fiber. The coupler has greater than 97.5% reflectance in the 450 nm-2μm range. The 200 μm optical fibers has a numerical aperture (NA) of 0.22 and low attenuation in the NIR. To protect the optical coupler from redeposition of sputtered material, a disposable protective 1 mm thick quartz window is placed over the optical coupler aperture.

The NIR optimized fiber optic patch cord from the optical coupler connects to a fiber optic vacuum feed through the chamber wall to a second patch cord coupled to the Horiba 1250M Series II spectrometer using a Horiba fiber optic adapter. The fiber adapter uses 100 mm and 30 mm lenses to focus light emitted from the fiber onto the spectrometer entrance slit. The spectrometer, with a 1.25 m focal length

(f/9), contains a 300 G/mm classically ruled diffraction grating, blazed at 500 nm, that produces a dispersion of 2.6 nm/mm. For the measurements presented here, the spectrometer entrance slit was fixed at 200 µm. While this limited the spectral resolution, it increased throughput for greater signal strength.

The emission spectrum is detected using a cooled Andor iStar® Intensified CCD (ICCD) with 1024 x 1024 pixels (13 µm x 13 µm) capable of dark currents as low as 0.065 e^-/pix/s. The camera intensifier system acts as a fast solid-state shutter capable of gating on 1 ns time scales. Gating is controlled by TTL input and user defined gate delay and gate width. The individually gated shots are accumulated over the length of the exposure and recorded using the National Instruments LabView PC based data acquisition system.

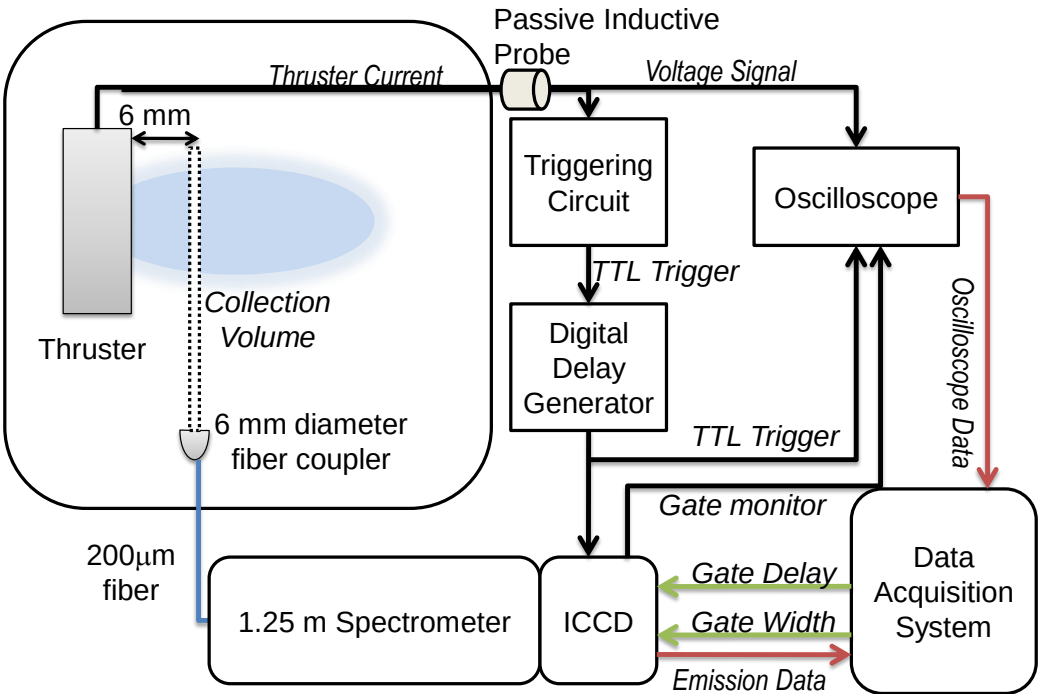

Figure 3: Optical system used to measure thruster emission using a 1.25m Horiba spectrometer with attached Andor ICCD. Emission measurements are triggered using a custom triggering circuit to synchronize measurements to current oscillations. Full breathing mode cycle is characterized by varying the delay between trigger and ICCD gating.

Emission measurements were background subtracted and wavelength calibrated using a standard xenon lamp. A relative spectral response (RSR) calibration was applied to correct for any wavelength dependence of emission detection due to the transmission losses introduced by the optical components. The RSR was determined using a NIST traceable 200 W tungsten filament standard of spectral irradiance and comparing the measured grey body emission to the ideal spectral response.

Timing and Triggering Circuit

A triggering system was developed to synchronize the ICCD gating with the oscillations in the discharge current. The peak of the discharge current served as a temporal reference for the breathing mode cycle and was used to trigger the gating of the ICCD. The temporal resolution was achieved by gating 1 µs

portion of the cycle and integrating over many cycles to ensure an adequate SNR. Measurement of the desired portion of the cycle was controlled by adjusting the delay between the reference discharge current peak and the ICCD gate. Characterization of the entire cycle was then achieved by varying the delay between reference discharge current peak and the ICCD gate trigger.

The trigger circuit uses analog components to process the discharge current signal into an ICCD trigger compatible transistor-transistor logic (TTL) output. Thruster current oscillations are measured using a passive inductive probe, which also incidentally acts as a band pass filter (3 dB points of 120 Hz and 20 MHz with < 1° phase shift at frequencies between 1-100 kHz). This low-level voltage signal is then passed through a low pass filter and subsequently differentiated, so that the zero crossings of the differentiated signal correspond to peak in the thruster anode current signal. Using a high-speed comparator acting as a zero crossing detector, a TTL signal is produced at the peak of the signal. A digital delay generator (DDG) is then used as a buffer between the triggering circuit and ICCD by filtering any false triggers caused by occasional inflection points in the discharge current.

To ensure gating is correctly synchronized to the desired portion of the signal, a 1 GS/s oscilloscope is used to monitor the thruster discharge current, the TTL trigger, and the ICCD gate monitor output. A sample oscilloscope trace is shown in Figure 4. The 2 μs delay between the minimum of the current signal and the trigger is caused by the delays added by the active circuit components and was found to be consistent in all measurements. After the trigger at time t = 9 μs, the ICCD delays gating for the input value of 13 μs. Additional delay added by ICCD electronics was found to be on the order of nanoseconds, and are assumed negligible. After gating for 1μs, the ICCD waits for the next TTL trigger to start the next cycle. The gated signals are accumulated by the ICCD until the end of the exposure. Measurement of the full breathing mode cycle is achieved by varying the gate delay from 0-26 μs. Time zero shown in subsequent figures will be defined at the fall of the TTL trigger, corresponding to an input gate delay of zero. A ± 0.2 μs uncertainty in the temporal resolution will be used based on the HWHM of the current FFT.

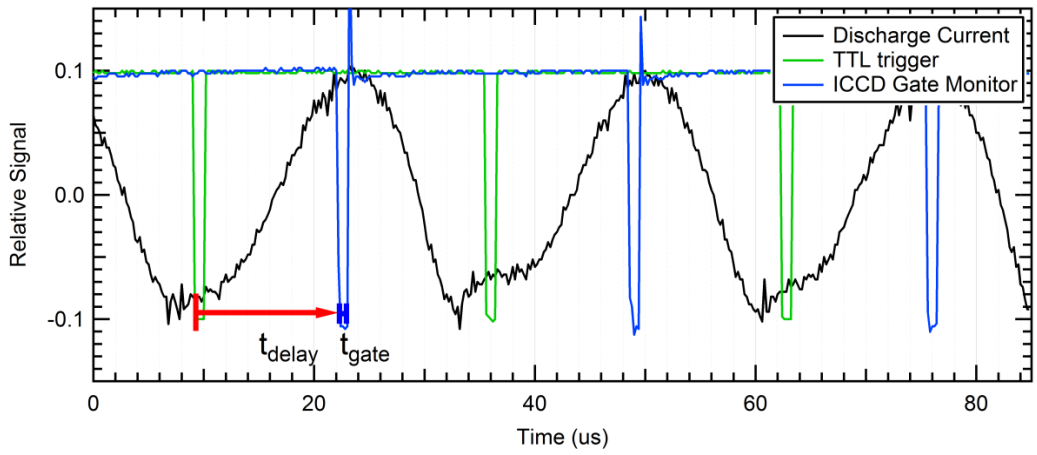

Figure 4: Sample oscilloscope trace with ICCD settings: 1 μs pulse width, 13 μs gate delay. Only 80μs of the 0.5 s exposure is shown.

Electron Temperature Measurements

Measurements were taken in the 810-840 nm NIR region to include the 823, 828, and 834 nm neutral xenon lines with a known relative intensity dependence on electron temperature. A collisional-radiative model (CRM) similar to the model developed by Karabadzhak et al.[17] is used to determine the electron temperature dependence of the line ratios. The KCD model uses empirical excitation cross sections and probability statistics to model Xe I metastable populations. The line intensity per unit volume can be approximated by:

$$J_{XeI}(\lambda) = \frac{hc}{4\pi\lambda}\left[N_0 N_e k_{eO}^{\lambda} + N_m N_e k_{em}^{\lambda} + N_0 N_1 k_{10}^{\lambda} + N_0 N_2 k_{20}^{\lambda}\right] \quad (1)$$

where N_i are the species number densities; k_{eO}^{λ} is the excitation rate coefficient for electrons with neutrals with emission at wavelength λ; k_{em}^{λ} is the emission excitation rate coefficient for electrons with metastables; and k_{10}^{λ} and k_{20}^{λ} are the emission excitation rate coefficient for Xe^{+} and Xe^{+2} ions with neutrals. Assuming quasineutrality, $N_e = N_1 + 2N_2$, and substituting $\alpha = N_1/N_e$, Equation (1) can be rewritten as

$$J_{XeI}(\lambda) = \frac{hc}{4\pi\lambda}(N_0 N_e)\left[k_{eO}^{\lambda} + \frac{N_m}{N_0} k_{em}^{\lambda} + \alpha\, k_{10}^{\lambda} + \frac{1-\alpha}{2} k_{20}^{\lambda}\right] \quad (2)$$

Rate coefficients are determined using:

$$k_{ij}^{\lambda} = \int_0^{\infty} f_i(E_i)\sigma_{ij}^{\lambda}(E_i)u_i\, dE_i \quad (3)$$

where $f_i(E_i)$ is the energy distribution of species i; $\sigma_{ij}^{\lambda}(E_i)$ is the excitation cross sections for a particle i, with energy E_i, with a particle j to produce emission at λ ; and u_i is the velocity of particle i. Excitation cross sections for neutral-electron and neutral-ion collisions are determined empirically from Chiu et al.[18] and Sommerville[19]. Assuming a Maxwellian electron energy distribution, k_{eO}^{λ} is determined as a function of the electron temperature, T_e. Rate coefficients k_{1O}^{λ} and k_{2O}^{λ} are determined assuming a uniform ion energy distribution. Cross sections for electron-metastable collisions have yet to be determined empirically. Therefore the excitation rate coefficient $k_{em}^{\lambda}$is approximated using the upper $2p_i$ level degeneracy and branching probabilities.

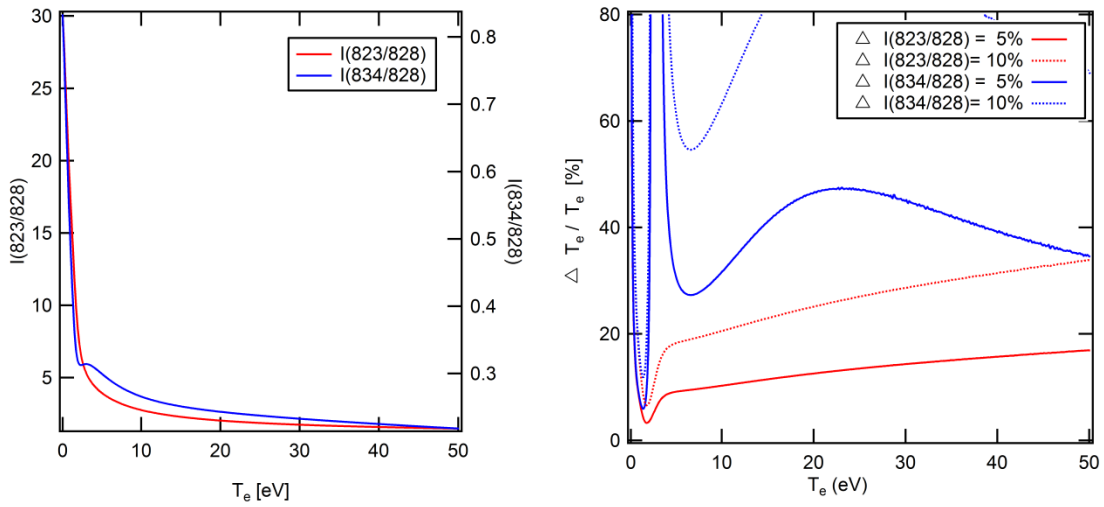

Figure 5: Left: Calculated intensity ratios as a function of electron temperature using the KCD model. Right: Uncertainties in electron temperature due to 5 and 10% uncertainty in line ratio.

Intensity ratios I_{823}/I_{828} and I_{834}/I_{828} are calculated using the KCD model are shown on the left in Figure 5. Ion species populations used in the model are from probe measurements by Nakles et al.[14] and Ekholm et al.[15] and ion velocity inputs are based on LIF data by Nakles et al.[16]. The discontinuity in the I_{834}/I_{828} line ratio near 2 eV is non-physical and is due to model approximation discontinuities. A parameter variation was done using a 20% increase in the Xe^{2+} population and a 10% increase in the ion velocity to determine their influence on the model. Both methods showed little sensitivity to the relative species populations or ion velocity, except in the low electron temperature regions where ion collisions play a more significant role.

Temperature uncertainties were based on 5% and 10% uncertainty in line intensity ratio. The resulting uncertainties are shown in Figure 5. The I_{823}/I_{828} ratio method appears more attractive due to its significantly lower temperature uncertainties, but this method relies on the metastable approximations for I_{823} line, which is not reflected in the temperature uncertainty. The I_{834}/I_{828} ratio method is more accurately modeled, but has significant uncertainties associated with intensity ratio uncertainties. Additionally, the I_{834} line is typically the lowest intensity of the three lines, resulting in lower SNR and higher line intensity ratio uncertainty. Therefore the I_{834}/I_{828} ratio method should not be used in conditions with low electron temperature or low emission signal.

III. Experimental Results

Emission Measurements

Emission measurements were taken 6 mm downstream of the thruster exit with a temporal resolution of 1 μs in the NIR (810-835 nm). The cooled ICCD achieved a high signal to noise ratio (SNR > 24 dB) for most cases. Emission measurements near minimum of the discharge current were difficult due to the low signal (SNR = 1.9 dB). Measurements were taken at gate widths of 1 μs accumulated over 0.5 s exposures (19,000 cycles). The emission spectra were background subtracted, wavelength calibrated, and RSR corrected.

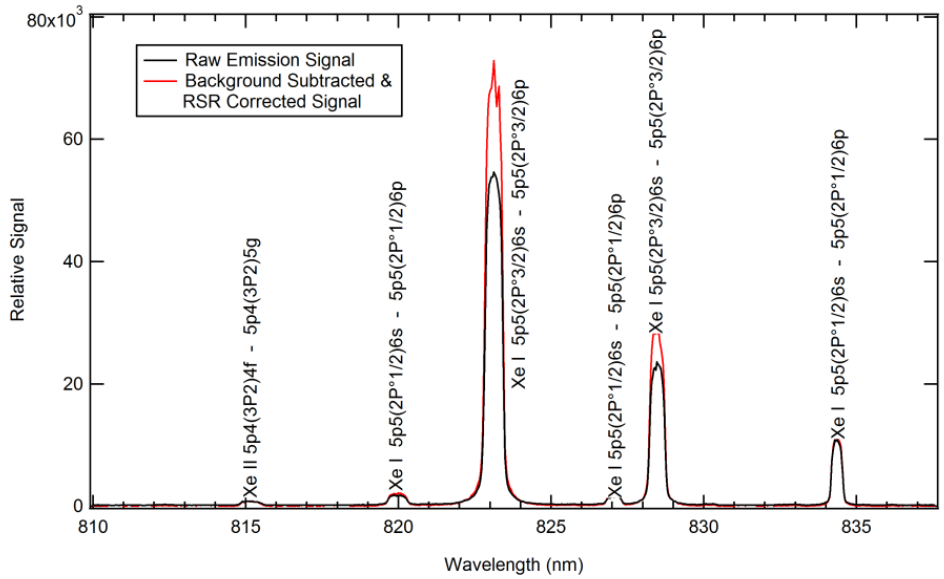

Figure 6: Sample emission spectrum of a BHT-600 at nominal operating conditions. Measurement taken near peak of discharge current oscillation with 1 μs gated shots over a 0.5 s exposure (19,000 cycles).

A sample emission spectrum is shown in Figure 6. A majority of the measured lines in this wavelength region are strong neutral lines. The emission from the metastable linked 823 nm line is the strongest of the three lines. The metastable state allows for excited neutrals with long lifetimes, which can then be easily re-excited producing strong emission lines. Additional neutral Xe lines are seen at 820 nm and 827 nm, but their low signal in proximity to the stronger lines makes them difficult to use for diagnostic purposes. This study focuses on the use of the three strongest lines (823, 828, and 834 nm) for determination of electron temperature.

The peak value normalized line intensities are shown in Figure 7 with a representative current trace. There is a strong correlation between the peak of the discharge current and the peak of the Xe neutral emission. Similar results were seen in a 200 W Hall thruster study by Liu et al[20] using high speed imaging to measure oscillations in visible emission with discharge current. A 2 μs delay is shown between the peak of the normalized intensity and the peak in the discharge current. Assuming this delay is based on the electron transit time between the measurement volume and the anode, an 8 ± 1 km/s average axial electron velocity can be approximated. A significant drop in emission signal is seen after 23 μs, near the minimum of the discharge current. The low signal in this portion of the cycle increased the uncertainty in line intensity measurements, especially for the lowest intensity line at 834 nm.

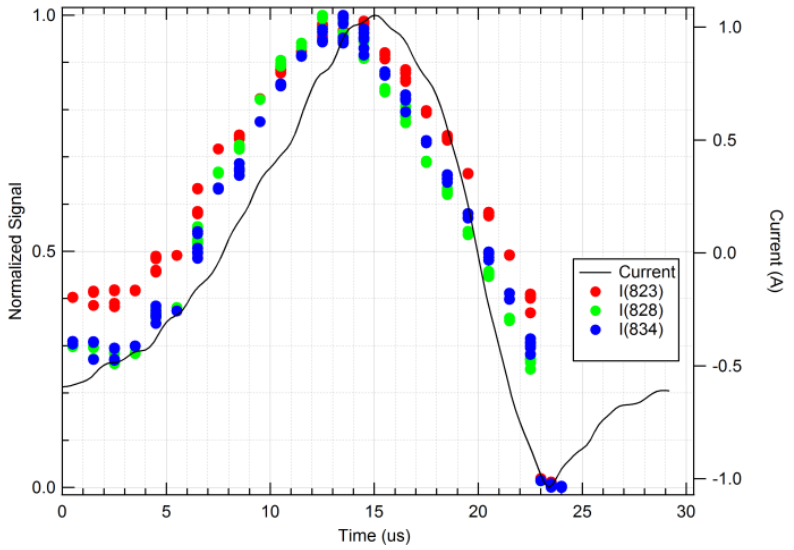

Figure 7: Normalized Xe I line intensities in comparison to discharge current. Measurements taken 6 mm downstream of thruster exit plane at nominal operating conditions. Due to low signal towards the end of the cycle, line intensities were unable to be determined.

Electron Temperature

Electron temperatures are determined using I_{823}/I_{828} and I_{834}/I_{828} line intensity ratios in conjunction with the results of the KCD model. The resulting electron temperatures are shown in Figure 8. The two methods are in general agreement, with electron temperatures fluctuating between 3-9 eV, -5 ± 1 μs out of phase with discharge current oscillations. The I_{823}/I_{828} ratio method results in average electron temperature of 6.6 ± 0.6 eV approximately -4 μs out of phase with discharge current. The I_{834}/I_{828} ratio method results in an average electron temperature of 6.2 ±1.8 eV, approximately -6 μs out of phase with discharge current. Higher scatter in the I_{834}/I_{828} versus the I_{823}/I_{828} ratio method is due to the I_{834}/I_{828} method's higher sensitivity to uncertainties in line ratio. Low signal at the end of the cycle (> 22 μs) lead to higher uncertainties with the integrated line intensity for all three lines, and therefore resulted in a higher uncertainty for both temperature methods.

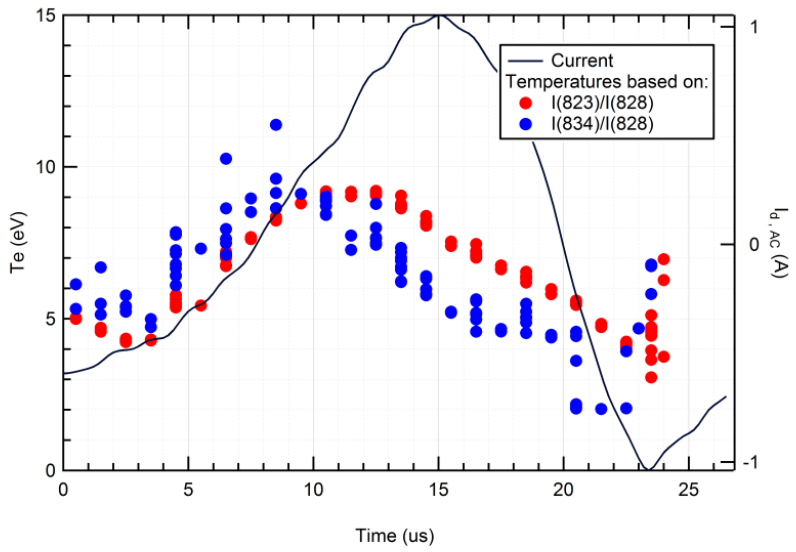

Figure 8: Electron temperature fluctuations 6 mm downstream of BHT-600 thruster exit plane at nominal operating conditions using the KCD model a two-line emission method.

IV. Numerical Model

The numerical model HPHall used in this study is a radial-axial hybrid particle-in-cell (PIC) model which is based on a fluid treatment of electrons and a PIC treatment of ions and neutrals as first developed by Fife[1]. Although simulations have been able to qualitatively reproduce the plasma oscillations seen experimentally in the "breathing mode" oscillations in discharge current[1-4], the lack of time-resolved data has made it difficult to validate. The goal of this numerical study is to characterize the breathing mode for comparison with time-resolved experimental data. Additionally, a sensitivity analysis is performed to determine the model's sensitivity to input conditions. Relevant details of the HPHall code are provided in this section but more complete references available[1-3].

Overview

The setup of all HPHall cases is based on neutral injection at nominal conditions (propellant injection temperature of 900 K and xenon mass flow rate of 2.45 mg/s), single and double ionization, inelastic collision effects (incorporated as an energy sink for the electron population), and anomalous collision effects (as a mechanism for calculating the electron mobility and electron energy losses). The electrostatic potential is calculated via a combination of current conservation and a generalized Ohm's law formulation for the electron current. The electron density is evaluated using an assumption of quasineutrality throughout the domain, the electrons are assumed to have zero inertia, and the electron energy is evaluated using an advection/diffusion equation with both sources (ohmic heating) and sinks (inelastic loss mechanisms).

The main limitation to this code is the lack of understanding of the mechanisms governing electron transport across the magnetic field lines. To account for this "anomalous" electron mobility, an effective mobility term is used. The effective mobility term used in HPHall modifies the classical mobility with a Bohm mobility term:

$$\mu_{\perp eff} = \mu_{\perp classical} + \mu_{Bohm} \tag{4}$$

$$\mu_{Bohm} = \frac{K_B}{16}\frac{1}{B} \tag{5}$$

where $K_B/16$ is referred to as the inverse Hall parameter. HPHall assumes an axially varying inverse Hall parameter, similar to that measured by Meezan et al.[21]. To determine the model's sensitivity to the choice of the inverse Hall parameter, simulations were run with varying inverse Hall parameter profiles as shown in Figure 9.

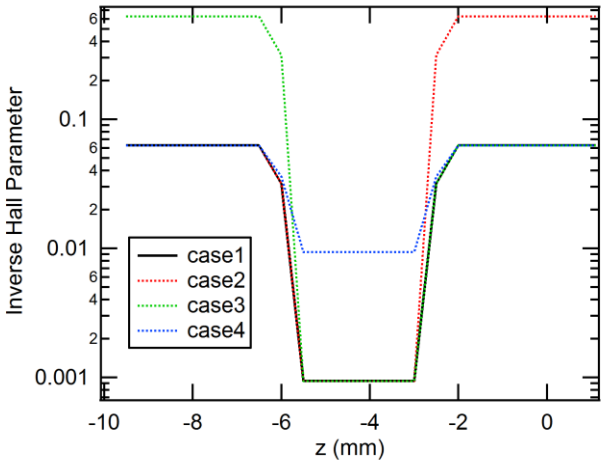

Figure 9: Inverse Hall parameter profiles used in simulation cases

V. Modeling Results

The simulations were run at a timestep of 0.25 μs over a 2 ms time period. A summary of the measured and simulated thruster performance is shown in Table 2. Measured thrust and I_{SP} performance metrics are based on published Busek values[13]. Electron temperature predictions from HPHall are based on an electron density weighted average of T_e evaluated in the emission collection volume. Oscillation magnitudes are estimated using a ratio of the standard deviation to the mean value.

Table 2: Comparison of HPHall predicted performance

	Units	Measured	HPHall Case 1	HPHall Case 2	HPHall Case 3	HPHall Case 4
T	mN	39	38	38	38	41
I_{SP}	s	1530	1530	1510	1530	1660
f_{BM}	kHz	38	34 ± 5	54 ± 5	31± 5	22 ± 5
$\bar{I}_d$	A	2.05	2.18	2.21	2.20	3.64
$\widetilde{I_d}/\bar{I}_d$	--	32%	7 %	11 %	7 %	6 %
$\bar{T}_e$	eV	6.6 ± 0.6	12.4	10.4	12.7	25.8

$\widetilde{T_e}/\overline{T_e}$	---	32 ± 8 %	4%	6%	4%	2%

Although the model was successful in predicting the overall thruster performance within 10% for all four cases, all cases had difficulty accurately modeling breathing mode behavior. Although most cases were able to predict average discharge current within 10%, all cases were significantly under the 32% oscillations measured in discharge current. Additionally, all simulations predicted higher than observed electron temperatures with significantly lower oscillation magnitudes.

Differences in the four cases can be seen in the breathing mode frequency, f_{BM}, indicating that breathing mode predictions are highly sensitive to choice of inverse Hall parameter profile. Changes in frequency appear to be non-linear, suggesting a complex relationship between the electron mobility and breathing mode frequency. Further analysis in this study will focus on Case 1, based on the compatibility of measured and Case 1 predicted values.

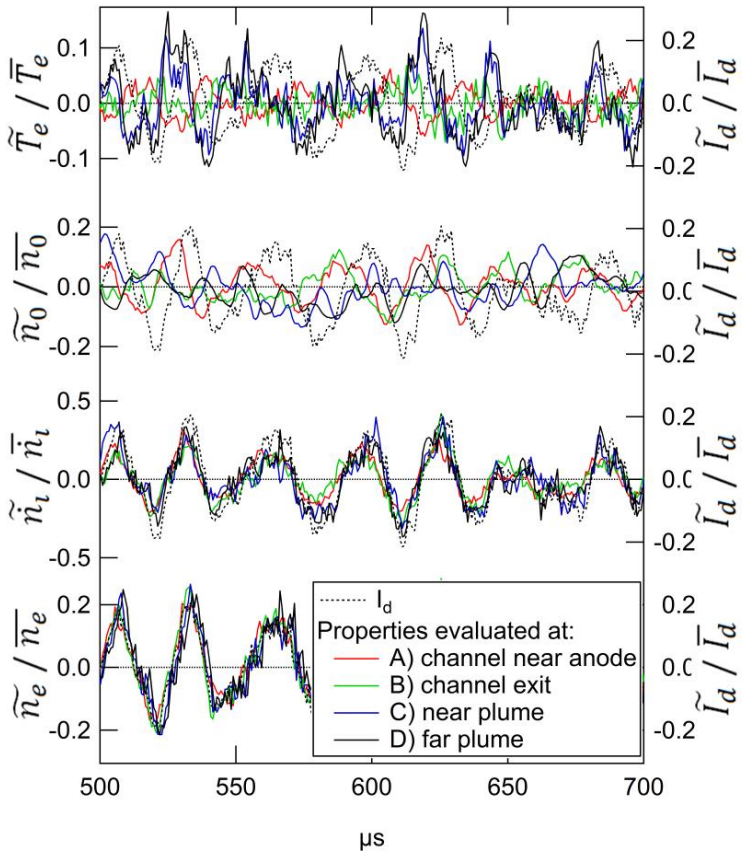

Figure 10: HPHall Case 1 predicted plasma property oscillations

Oscillations in plasma properties were sampled at four axial locations: A) channel near anode (-5 mm), B) channel exit (0 mm), C) near plume (6 mm), and D) far plume (15 mm). Fluctuations in neutral population, ionization rate, electron density, and electron temperature are shown in Figure 10. Cross-correlations of the plasma properties with the discharge current in shown in Figure **11Error! Reference**

source not found.. The cross-correlation is determined by evaluating the correlation coefficient R between the discharge current and the plasma property, while varying the delay (τ) to the plasma property.

$$R(\tau) = [\sum(X_t - \bar{X})(Y_{t+\tau} - \bar{Y}) \ ] \ / \ [\sum(X_t - \bar{X}) \sum(Y_{t+\tau} - \bar{Y}) \ ] \quad (6)$$

The peak of the correlation coefficient is used to determine the delay between the discharge current and the plasma property.

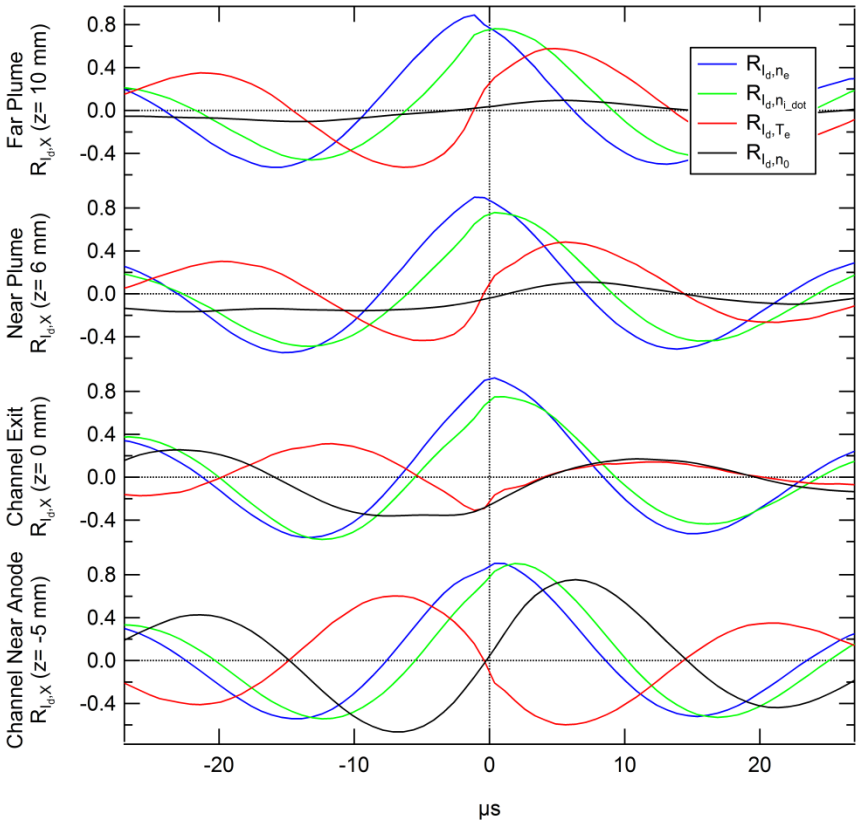

Figure 11: HPHall Case 1 cross-correlations of plasma properties with discharge current

A summary of the predicted fluctuations is shown in Table 3. The magnitudes of the oscillations are estimated using ratio of the standard deviation to the mean value. Breathing mode frequency is determined using frequency analysis, with an uncertainty of ±5 kHz based on the HWHM of the spectrum peak. Delays were determined using the peak of the cross-correlation. An uncertainty of ± 1μs is based on the accuracy of the cross correlation method. The phase shift, $\boldsymbol{\phi_{Ix}}$, is determined as a ratio of the delay to the oscillation period, expressed in degrees. Low confidence values, correlation coefficient (R<0.30), are shown in blue italics.

Table 3: Summary of HPHall Case 1 predicted plasma property fluctuations

	Axial Location	$\bar{x}$	$\frac{\tilde{x}}{\bar{x}}$	freq (kHz)	τ_{delay} (μs)	$\phi_{I_d,x}$ (degrees)	R
I_d	--	2.2 A	7%	34	--	--	1.00
n_0	A	9.5E+18 m^{-3}	4%	33	6.4	77	0.75
	B	2.1E+18 m^{-3}	5%	33	*-22.9*	*-275*	*0.26*
	C	5.6E+17 m^{-3}	7%	28	*7.1*	*73*	*0.11*
	D	3.9E+17 m^{-3}	7%	33	*5.6*	*68*	*0.09*
$\dot{n}_\iota$	A	1.2E+24 m^{-3}	8%	33	1.9	23	0.90
	B	1.7E+23 m^{-3}	9%	34	1.1	14	0.75
	C	1.9E+22 m^{-3}	12%	34	0.4	5	0.76
	D	6.3E+21 m^{-3}	13%	33	0.4	5	0.76
n_e	A	1.1E+18 m^{-3}	7%	34	0.4	5	0.91
	B	6.4E+17 m^{-3}	8%	34	0.4	5	0.93
	C	3.5E+17 m^{-3}	8%	34	-1.1	-14	0.90
	D	2.4E+17 m^{-3}	9%	33	-1.1	-14	0.89
T_e	A	27.3 eV	2%	34	-7.1	-87	0.60
	B	23.0 eV	2%	34	-11.6	-143	0.31
	C	16.5 eV	4%	34	5.6	68	0.48
	D	12.5 eV	5%	34	4.9	59	0.58

Although the predicted phase shifts vary across axial locations, the general trends are in agreement with the predator prey theory and experimental data. Simulations are consistent with predator prey theory of a periodic depletion of neutrals coupled with the increased ionization and plasma density. Additionally, predicted phase shifts between electron temperature and discharge current for the near plume (Location C) are in excellent agreement with observations ($-68^{\circ} \pm 14^{\circ}$). Although the model was able to capture the phase trends, simulations greatly under predict the magnitude of oscillations in comparison to the observed discharge current and electron temperature. Oscillations are also significantly lower than the 53.5% ± 9.8 % observed by Lobbia et al.[10,11].

VI. Conclusions

New time-resolved methods have been developed to gain understanding of the complex dynamics of the Hall thruster breathing mode. Time resolved (1μs) emission measurements were taken of the near plume using a high speed, gated ICCD. The I_{823}/I_{828} and I_{834}/I_{828} line intensity ratios were used in

conjunction with the KCD collisional radiative model to determine electron temperature. Electron temperatures in the near plume were found to fluctuate between 3-9 eV. A strong correlation between the discharge current and electron temperature was observed with a significant phase shift (-68°) between cycles.

Simulations were performed using HPHall and compared with experimental data to validate the model's breathing mode predictions. Although the model was able to correctly estimate the time averaged performance metrics, the model had difficultly modeling the more complex breathing mode oscillations. Differences in breathing mode frequency between the simulation cases emphasize the model's sensitivity to choice of inverse Hall parameter profile. Although the general phase trends of the model are in agreement with predator prey theory and experimental data, the simulations greatly under predict the magnitude of the oscillations. Additionally, the simulations predict higher than observed electron temperatures.

One issue with the current model is the decoupling of the plasma dynamics and Bohm mobility. HPHall attempts to capture the turbulent mobility in the effective mobility with the additional of a fixed Bohm mobility term. The Bohm mobility profiles were selected through an iterative process designed to capture accurate steady state thruster behavior (including the discharge potential and current), but the fixed profiles fail to capture dynamic thruster behavior. Also by imposing a fixed mobility, it is effectively damping the oscillations of the system. Additionally, this causes a higher than observed electron temperature as the model attempts to maintain the target discharge current. In reality, the turbulent mobility is coupled with oscillating plasma dynamics and therefore some interplay is expected on the 10-100 kHz timescale between the plasma density and mobility profile. Furthermore, the model cannot be expected to accurately reflect the full range of electron mobility without a time-dependent electron dynamics model to inform the Bohm mobility. Future work is needed to understand the complex relationship between the breathing mode and electron mobility, and how best to develop efficient models to predict thruster dynamics.

VII. Acknowledgements

The authors would like to thank Dr. Michael Holmes and Paul Adkison for their assistance with development of the triggering system, as well as Michael Nakles for his assistance with the experimental work.

References

1. Fife, John M. *Hybrid-PIC Modeling and Electrostatic Probe Survey of Hall Thrusters.* PhD Thesis, Massachusetts Institute of Technology, 1998.

2. Parra, F.I., E. Ahedo, J.M. Fife, and M. Martinez-Sanchez. "A two-dimensional hybrid model of the Hall thruster discharge." *Applied Physics*, 2006: 023304-1.

3. Hofer, R.R, I. Katz, I.G. Mikellides, and M. Gamero-Castano. "Heavy Particle Velocity and Electron Mobility Modeling in Hybrid-PIC Hall Thruster Simulations." *42nd AIAA/ASME/SAE/ASEE Joint Propulsion Conference & Exhibit* AIAA-2006-4658.

4. Barreilles, J., G.J.M Hagelaar, L. Garrigues, C. Boniface, and J.P. Boef. "Critical assessment of a two-dimensional hybrid Hall thruster model:Comparisons with experiments." *Physics of Plasmas*, 2004: 3035.

5. Koo, J.W. *Hybrid PIC-MCC Computational Modeling of Hall Thrusters.* PhD Thesis, The University of Michigan, 2005.

6. Nakles, M.R., L. Brieda, G. Reed, W.A. Hargus, and R.L. Spicer. "Experimental and Numerical Examination of the BHT-200 Hall Thruster Plume." *43rd AIAA/ASME/SAE/ASEE Joint Propulsion Conference* AIAA 2007-5305.

7. Scharfe, M.K., N. Gascon, and M.A. Cappelli. "Comparison of hybrid Hall thruster model to experimental measurements." *Physics of Plasmas*, 2006: 083505-1.

8. Boeuf, J. P.; Garrigues, L. , "Low frequency oscillations in a stationary plasma thruster," *Journal of Applied Physics* , 1998: 3541.

9. Choueiri, E. Y. ,"Plasma oscillations in hall thrusters," *Physics of Plasmas*, vol. 8, no. 4, pp. 1411–1426, April 2001.

10. Lobbia, R.B. *A Time-resolved Investigation of the Hall Thruster Breathing Mode.* PhD Thesis, Univeristy of Michigan, 2010.

11. Lobbia, R.B., and A.D Gallimore. "High-speed dual Langmuir probe." *Review of Scientific Instruments*, 2010: 073503.

12. Gonzales, A.E., W.A. Hargus, and M.R. Nakles. "Non-Intrusive, Time-Resolved Hall Thruster Near-Field Electron Temperature Measurements." *47th AIAA/ASME/SAE/ASEE Joint Propulsion Conference and Exhibit* AIAA-2011-5587 .

13. Busek Co. *Busek Low Power Hall Thrusters Data Sheet.* http://www.busek.com/index_htm_files/70008510.pdf.

14. Karabadzhak, G.F., Y. Chiu, and R.A. Dressler. "Passive optical diagnostic of Xe propelled Hall thrusters.II. Collisional-radiative model." *Journal of Applied Physics*, 2006: 113305.

15. Chiu, Y., B.L. Austin, S. Williams, R.A. Dressler, and G.F. Karabadzhak. "Passive optical diagnostic of Xe-propelled Hall thrusters.I. Emission cross sections." *Journal of Applied Physics*, 2006: 113304.

16. Sommerville, J.D. *Emission Cross Sections for Neutral Xenon Impacted by Xe+ and Xe2+*. PhD Thesis, Michigan Technological University, 2006.

17. Nakles, M.R., R.R. Barry, C.W. Larson, and W.A. Hargus. "A Plume Comparison of Xenon and Krypton Propellant on a 600 W Hall Thruster." *31st International Electric Propulsion Conference*, 2009.

18. Ekholm, J.M., W.A. Hargus, W. Larson, M.R. Nakles, G. Reed, and C.S. Niemela. "Plume Characteristics of the Busek 600 W Hall Thruster." *42nd AIAA/ASME/SAE/ASEE Joint Propulsion Conference* AIAA 2006-4659.

19. Nakles, M.R., and W.A. Hargus. "Background Pressure Effects on Internal and Near-field Ion Velocity Distribution of the BHT-600 Hall Thruster." *44th AIAA Joint Propulsion Conference*, 2008.

20. Liu, D., R.E. Huffman, R.D. Branam, and W.A. Hargus. "Ultra-High Speed Imaging of Hall ThrusterDischarge Oscillations with Krypton Propellant." *IEEE Transactions on Plasma Science*, 2011: 2926.

21. Meezan, N.B. *Electron Transport in a Coaxial Hall Discharge.* PhD Thesis, Stanford University, 2002.